NOTES AND CORRESPONDENCE

Single-Doppler Radar Observations of a Mini-Supercell Tornadic Thunderstorm

PATRICK C. KENNEDY

Department of Atmospheric Science, Colorado State University, Fort Collins, Colorado

NANCY E. WESTCOTT AND ROBERT W. SCOTT

Illinois State Water Survey, Champaign, Illinois

16 April 1992 and 20 October 1992

ABSTRACT

During the early evening hours of 19 May 1989, the CHILL 10-cm Doppler weather radar observed most of the lifetime of an unusually small tornadic thunderstorm. Throughout the event, the parent thunderstorm echo top remained below 6.7 km MSL. The low-altitude echo diameter, as defined by the 25-dBZ contour, was only 15 km. Despite its small size, both visual and radar observations indicated that this storm contained many of the organizational features often noted in large, "classical" southern Great Plains supercells. The synoptic setting in which this storm occurred was atypical for supercell development in that both the thermodynamic instability and vertical wind shear magnitudes were limited. This documentation of a tornadic storm that developed in a nonthreatening environment and that presented a small, seemingly inconsequential radar appearance demonstrates some of the challenges that will be faced by automated Doppler radar–based severe weather detection algorithms.

1. Introduction

A primary motivation for the installation of a national network of Doppler weather radars (WSR-88D) is to improve tornado detection capabilities and to increase warning lead times. The realization of these benefits is crucially dependent upon the correct recognition of tornado-related rotation signatures in the radial velocity data. Thunderstorm research results from the southern Great Plains indicate that the development of a midlevel mesocyclone and its subsequent descent often precede the touchdown of a major tornado (JDOP staff 1979). Important variations to this genesis pattern exist, however. Wakimoto and Wilson (1989) presented evidence that the interaction of a developing thunderstorm with preexisting shear instability in the boundary layer can produce a tornado circulation that grows upward from the surface. In addition, outflows from mature storms have been found to be capable of generating tornadoes along the edges of gust fronts and downbursts (Forbes and Wakimoto 1983). This variety of developmental sequences can make Doppler radar recognition of tornadic storms difficult. The purpose of this note is to expand the spectrum of Doppler radar–observed tornadic thunderstorms through the documentation of an unusually small tornadic storm and the synoptic setting in which it occurred.

Corresponding author address: Patrick C. Kennedy, Department of Atmospheric Science, Colorado State University, Fort Collins, CO 80523.

2. Case description

a. The synoptic setting

Several periods of thunderstorms, some of which were severe, occurred in central Illinois beginning in the late morning hours of 19 May 1989. By 1900 (all times are CDT), most of the thunderstorm activity had moved into western Indiana and it appeared that the severe weather threat in central Illinois had ended. Nevertheless, a tornado developed and touched down at 2007 near the town of Bement, 30 km southwest of the CHILL radar site at the University of Illinois Willard Airport, Champaign (CMI). (See Fig. 1a for geographic references.)

At 1900, a developing warm front was advancing eastward at approximately 10 m s^{-1} across the western third of Illinois (Fig. 1a). The wind shift along this boundary was well defined, but surface temperatures were only 2°C warmer west of the front. No significant surface moisture convergence was diagnosed in the vicinity of the front.

A trough associated with the warm front was apparent at the 850-mb level (Fig. 1b). At this level, most

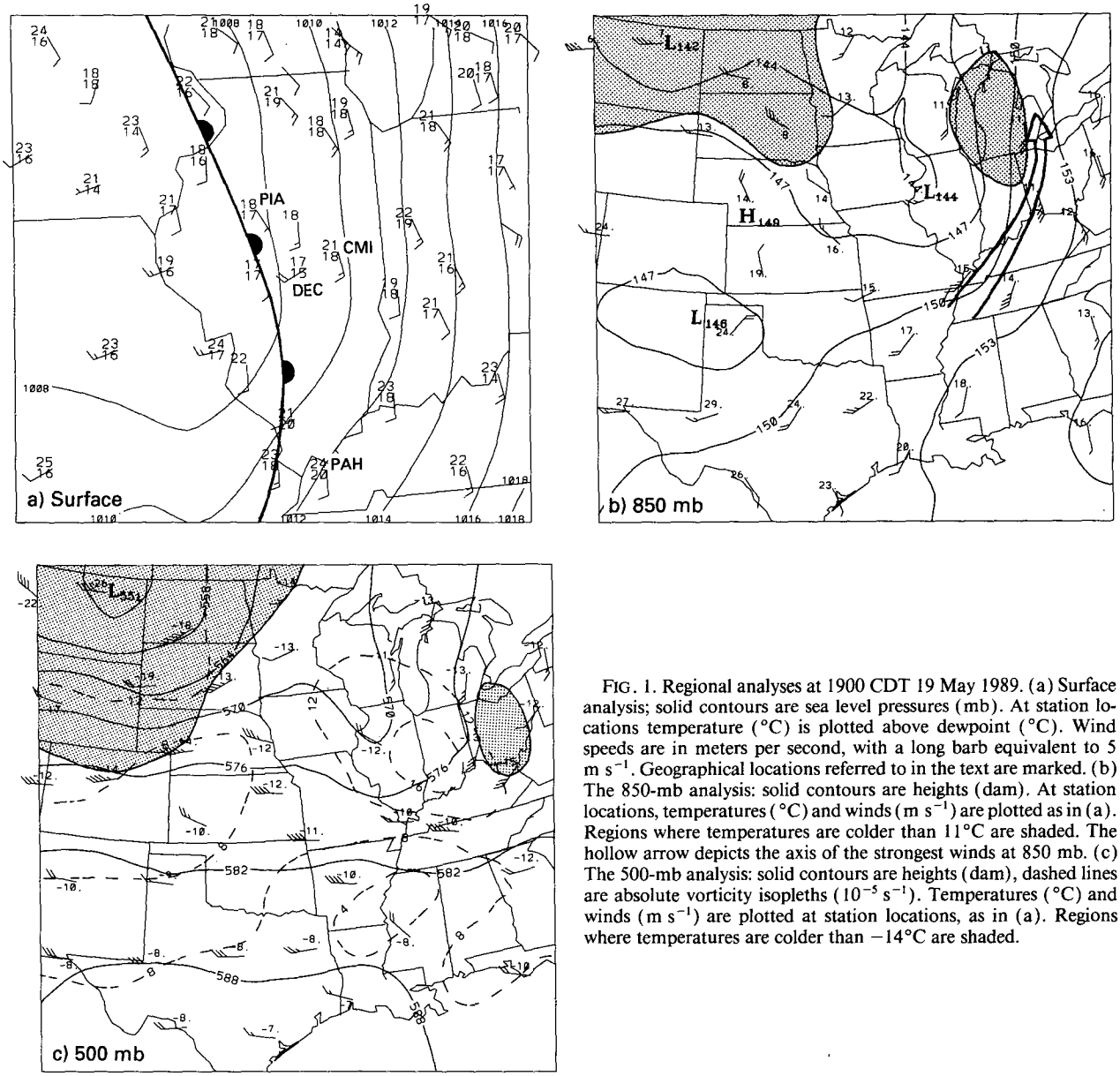

FIG. 1. Regional analyses at 1900 CDT 19 May 1989. (a) Surface analysis; solid contours are sea level pressures (mb). At station locations temperature (°C) is plotted above dewpoint (°C). Wind speeds are in meters per second, with a long barb equivalent to 5 m s^{-1}. Geographical locations referred to in the text are marked. (b) The 850-mb analysis: solid contours are heights (dam). At station locations, temperatures (°C) and winds (m s^{-1}) are plotted as in (a). Regions where temperatures are colder than 11°C are shaded. The hollow arrow depicts the axis of the strongest winds at 850 mb. (c) The 500-mb analysis: solid contours are heights (dam), dashed lines are absolute vorticity isopleths (10^{-5} s^{-1}). Temperatures (°C) and winds (m s^{-1}) are plotted at station locations, as in (a). Regions where temperatures are colder than −14°C are shaded.

of the synoptic-scale support for convective activity was found east of Illinois; the analysis suggested the presence of a low-level jet extending from Memphis through Louisville to Detroit. Upward vertical motion was strongest in the area between Memphis and Indianapolis based on the convergence of **Q** vectors (Hoskins et al. 1978; not shown). Also, the coldest temperatures at 850 mb were centered ahead of the trough axis over lower Michigan.

A generally similar pattern existed at 500 mb (Fig. 1c). The trough axis persisted across east-central Illinois, with the coldest temperatures located well to the east over the Ohio River valley. An objective analysis placed a vorticity maximum just southeast of CMI. Although the vorticity magnitude was fairly high over eastern Illinois (16×10^{-5}–18×10^{-5} s^{-1}), vorticity advection was limited due to the weak 500-mb wind speeds.

The presence of a vorticity maximum was confirmed by the comma pattern seen in the 1931 visible satellite image (Fig. 2). Based on the comma configuration, the vorticity center was located roughly 80 km northwest of the position analyzed at 500 mb. While this would imply greater positive vorticity advection (PVA) over CMI than indicated by the 500-mb objective analysis, any PVA that existed was probably weak. Also apparent in the image are the arc of deep convective clouds from western Indiana to southern Illinois and the isolated storm that was responsible for the Bement tornado.

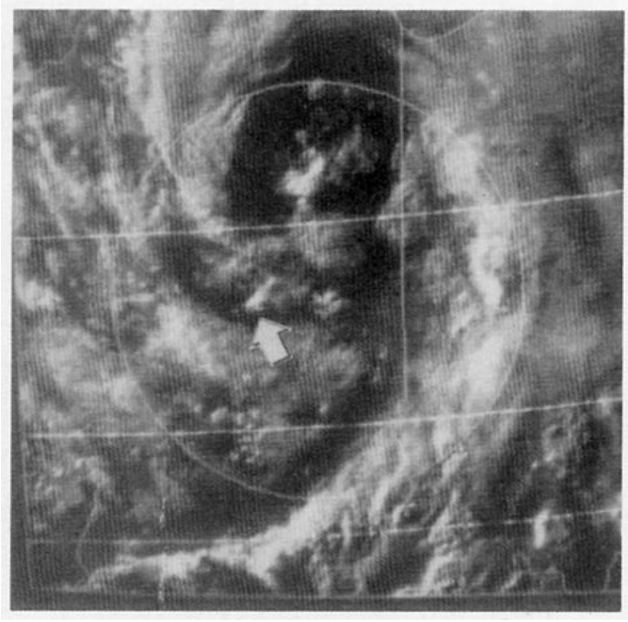

FIG. 2. GOES 1-km resolution visible image at 1931 CDT 19 May 1989. The tornadic storm cloud is marked with an arrow. The range ring is 150 km from the radar.

The horizontal distribution of thermodynamic instability at 1900 was related to the satellite-observed cloud pattern. Near the arc of deep convection in southern Illinois, moderate instability was present in the National Weather Service (NWS) Paducah, Kentucky, (PAH) sounding (not shown). The lifted index[1] for PAH was −3 and the K index[2] was 36. In the tornado environment behind the convective line, less instability was present in the NWS Peoria, Illinois, (PIA) sounding where the lifted and K indices were 0 and 30, respectively (Fig. 3). Except in the vicinity of the stable layer near 550 mb, the PIA sounding was moist.

Some sense of the severe weather threat level implied by the Bement tornado's environment may be gained through the consideration of Miller's (1972) checklist. This list tabulates selected synoptic-scale parameters that are most applicable to categorizing the spring season severe weather threat level. Following Maddox and Doswell (1982), a simplified version of Miller's severe weather parameters for the Bement tornado is presented in Table 1. In this case, Miller's parameters were split fairly evenly between the weak and moderate categories; none of the parameters could be classified as strong. With the exception of the 300- and 200-mb wind speeds, all of the moderate category parameters were related to the low-level pressure and moisture fields. Most of the parameters related to the intensity of the synoptic-scale dynamics (500-mb wind speed, PVA, 12-h height change, etc.) were diagnosed as weak.

The helicity (H) and convective bulk Richardson number (BRI) properties of Bement tornado environment, as reflected by the 1900 PIA sounding, were also analyzed.

Helicity has been suggested as a severe weather forecasting tool in the sense that large helicities are conducive to the formation of mesocyclones and tornadoes (Davies-Jones et al. 1990). As interpreted by these authors, helicity can be related to the area swept out on a hodograph between the surface and 3 km AGL by the storm-relative wind vector. The motion of the Bement storm (from 269° at 8.7 m s^{-1}) was quite close to the mean wind in the lowest 4 km of the PIA sounding, implying limited helicity (Fig. 4). The helicity value was calculated using the formula presented by Davies-Jones et al. (1990):

$$H = \sum_{n=0}^{N-1} [(u_{n+1} - c_x)(v_n - c_y) - (u_n - c_x)(v_{n+1} - c_y)], \quad (1)$$

where $u_0 - u_N$ and $v_0 - v_N$ are the observed wind components at heights between the surface and $n = N$ (3 km AGL); and c_x, c_y are the storm-motion components. An evaluation of H based upon the PIA wind profile and the observed storm motion yielded a distinctly low helicity of some 20 m^2 s^{-2}. This value may be compared with the results of Davies-Jones et al. (1990). Based upon their examination of the National Severe Storms Laboratory archives, they found that the helicity ranges for weak, strong, and violent tornado categories were roughly 150–299, 300–449, and greater than 450 m^2 s^{-2}, respectively.

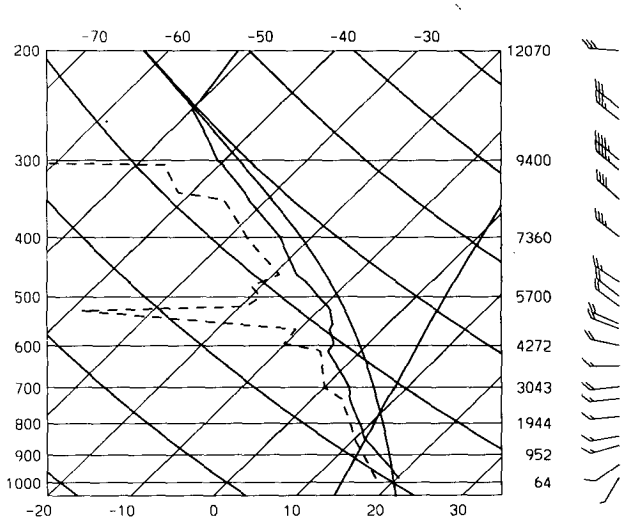

FIG. 3. Skew T–log$p$ plot of the 1900 CDT 19 May 1989 PIA NWS sounding. Only single moist adiabat and saturation mixing ratio lines are shown. Wind speeds are in meters per second, with a long barb representing 5 m s^{-1}.

[1] In this lifted-index computation, the parcel LFC (level of free convection) is based on the mean potential temperature and mixing ratio in the lowest 100 mb of the sounding.

[2] The K index is defined as (T850 − T500) + [T_d850 − (T700 − T_d700)], where T850 is the 850-mb temperature and T_d850 is the 850-mb dewpoint temperature, etc.

TABLE 1a. Summary of key synoptic parameters (after Maddox and Doswell 1982).

Rank	Parameter	Weak (W)	Moderate (M)	Strong (S)
1	500-mb vorticity advection	neutral or NVA	PVA: ≤30° height–vorticity contour crossing angle	PVA: >30° height–vorticity contour crossing angle
2	stability totals index (°C)	TI ≤ 50	50 < TI ≤ 55	TI > 55
3	500-mb wind speed (m s^{-1})	WS ≤ 18	18 < WS ≤ 25	WS > 25
4	300–200-mb wind speed (m s^{-1})	WS ≤ 28	28 < WS ≤ 43	WS > 43
5	850-mb wind speed (m s^{-1})	WS ≤ 10	10 < WS ≤ 18	WS > 18
6	850-mb dewpoint (°C)	$T_d \leq 8$	$8 < T_d \leq 12$	$T_d > 12$
7	850-mb temperature ridge location	east of moist axis	over moist axis	west of moist axis
8	700-mb 12-h temp, no change line	winds cross line ≤20°	winds cross line between 20° and 40°	winds cross line >40°
9	700-mb dry intrusion	not available or weak 700-mb winds	winds from dry to moist intrude at <40° angle and are >7.5 m s^{-1}	dry to moist winds intrude at ≥40° angle and are ≥13 m s^{-1}
10	12-h surface pressure fall (mb)	<1	1 to 5	>5
11	12-h 500-mb height change (m)	<30	≥30 and ≤60	>60
12	threat area surface pressure (mb)	≥1010	<1010 and ≥1005	<1005
13	surface dewpoint (°C)	$T_d \leq 13°$	$13 < T_d \leq 18$	$T_d > 18$

The smallness of the convective BRI has been used by Weisman and Klemp (1984) to identify environments conducive to supercell formation. In particular, their numerical modeling studies indicated that supercell organization was favored by BRI values less than 25–30. Following Weisman and Klemp (1984), the sounding convective available potential energy was obtained from

$$\text{CAPE} = g \int \frac{\theta(z) - \bar{\theta}(z)}{\bar{\theta}(z)}\, dz, \qquad (2)$$

where the integral was taken over the area of the sounding in which the potential temperature of a representative boundary-layer parcel undergoing moist-adiabatic ascent (θ) exceeded that of the surrounding environment ($\bar{\theta}$). The BRI was then given by

$$\text{BRI} = \frac{\text{CAPE}}{\frac{1}{2}(\bar{u}^2 + \bar{v}^2)}, \qquad (3)$$

where $\bar{u}$ and $\bar{v}$ are the components of the vector difference between the boundary-layer wind and the density-weighted mean wind though a specified lower-tropospheric depth.

As will be shown in the radar analysis section, the top of Bement storm was low (6 km MSL). Due to

TABLE 1b. Key parameter of evaluations for Bement tornado case.

Rank	Parameter	Bement case	Miller (1972) category
1	500-mb PVA	neutral/NVA	weak
2	stability totals index	45.1°C	weak
3	500-mb wind speed	10 m s^{-1}	weak
4	300–500-mb wind speed	23 m s^{-1}	moderate
5	850-mb wind speed	7.5 m s^{-1}	weak
6	850-mb dewpoint	10°C	moderate
7	850-mb temperature ridge location	Not applicable (temperature trough over moist ridge)	
8	700-mb, no change line	Not applicable (no change line well north of area)	
9	700-mb dry intrusion	none	weak
10	12-h surface pressure fall	~2.5 mb	moderate
11	12-h 500-mb height change	−10, +30	weak
12	surface pressure	1008 mb	moderate
13	surface dewpoint	17°C	moderate

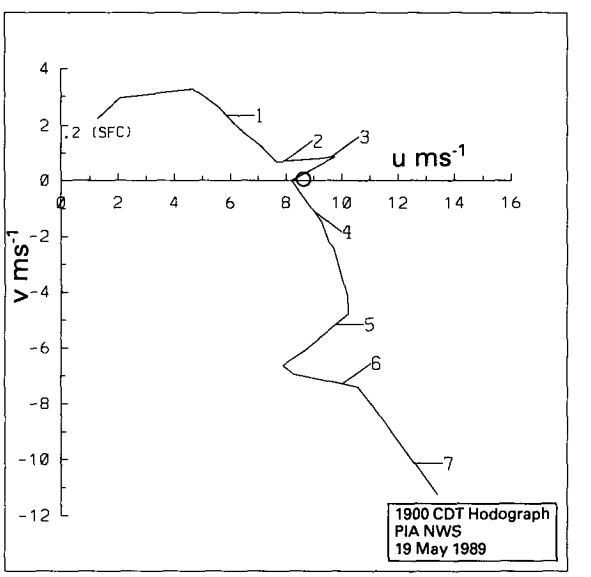

FIG. 4. Hodograph of the 1900 CDT 19 May 1989 PIA NWS sounding winds through the approximate depth of the storm. Heights are in kilometers MSL, wind speeds are in meters per second. The storm motion (from 269° at 8.7 m s^{-1}) is marked with an open circle.

the shortness of the storm, the appropriate depth through which the vertical wind shear in the BRI denominator should be calculated is probably less than the 6-km value used by Weisman and Klemp (1984). For shear depths between 4 and 6 km, the BRI in the PIA data was found to lie between 45 and 23, that is, in the upper portion of the supercell range. These relatively low values were due to the balance between the sounding's limited convective available potential energy (approximately 350 $m^2 s^{-2}$) and weak vertical wind shear (9 $m^2 s^{-2}$ through a 4-km depth and 17 $m^2 s^{-2}$ for a 6-km-deep layer).

From both the helicity and BRI perspectives, the 1900 PIA sounding was unlike the "classic" unstable, energetic tornado environment. These differences call into question the representativeness of the PIA sounding. This sounding was the closest one to the tornado in space and time (within 120 km and 2 h). Nevertheless, the surface and upper-air analyses both indicate that some differences probably existed between PIA sounding and the true near-storm environment. In particular, these synoptic analyses indicate that both at the surface and aloft the southerly flow component was likely stronger near the storm than in the PIA vicinity. Helicities based on wind profiles modified to plausibly reflect the storm environment did not exceed 105 $m^2 s^{-2}$. Thus, while the PIA data probably underestimated the tornadic potential, it appears that at best the environment was only weakly supportive of tornado development.

b. *The tornado*

The Bement tornado was small, occurred near dusk, and tracked through rural areas, so eyewitness observations were incomplete. Damage surveys were only made at a few points along the storm path, so details of the track are unknown. Several locations where surface damage was reported, however, were closely associated with the observed path of the circulation couplet pattern observed in the low-elevation-angle Doppler data. In this study, tornado locations and times were taken from severe weather warnings and statements issued by the Springfield, Illinois, NWS office, from local newspaper reports, and from sightings by law enforcement personnel.

Based on NWS reports, the tornado was preceded by a funnel cloud sighted at 1912 near the north side of Decatur (DEC). The tornado touched down at 2007 just south of Bement, and apparently dissipated approximately 25 min later. The track of the centroid of the parent mesocyclone is shown in Fig. 5. Eyewitness observations indicate that both the tornado and the parent thunderstorm remained quite small during their lifetimes. The visual aspects of the storm bore a marked resemblance to a "midget supercell" observed by Davies (1990) in central Kansas. As in the Kansas case, several features usually seen in larger, southern Great Plains tornadic storms were present (Moller 1978). In particular, the tornado appeared beneath a lowered portion of a visually rain-free cloud base located southwest of the heavy precipitation core (Fig. 6). Virtually all of the tornado's 19-km-long path crossed open farmland; some power lines were downed and F0 to F1 damage (Fujita 1981) was done to the few structures that were affected. Except for the Bement tornado, no other severe weather was reported in east central Illinois during the evening hours of 19 May 1989.

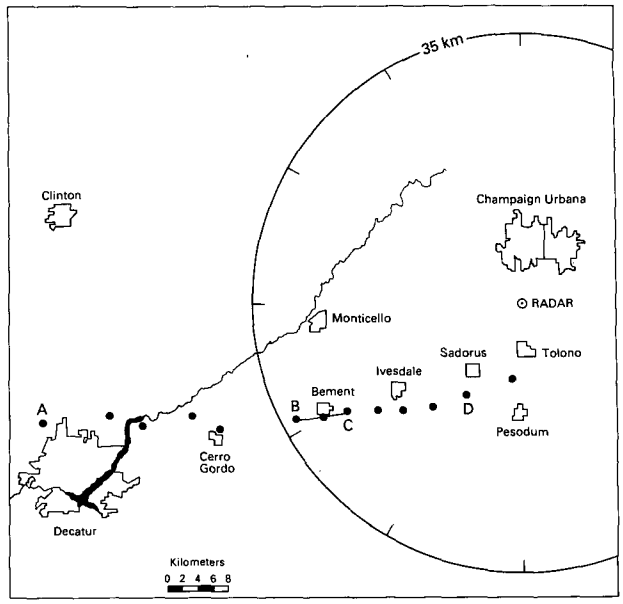

FIG. 5. Track of the centriod of the low-elevation-angle Doppler velocity couplet. Events marked by letters along the track are as follows: (a) 1910:21 CDT, funnel cloud reported at approximately 1912; (b) 2006:03, tornado touchdown reported at approximately 2007; (c) 2016:34, estimated tornado location at the time when the Fig. 6 photograph was taken; and (d) 2040:25, last point of significant damage along the tornado track.

3. Echo morphology

Supercell thunderstorm echoes have been observed to follow a fairly well-defined life cycle. Summaries of a "classical" supercell's life cycle have recently been made by Ray (1990) and Burgess and Lemon (1990). The normal sequence of events reported in these summaries is as follows.

1) The supercell begins with an undistinguished, often multicellular structure. These initial reflectivity cores are vertically aligned, and the storm moves with the mean wind in the echo-bearing layer.

2) Approximately 1 h into the storm's life, a strong, steady updraft begins to develop on the right flank of the storm. The existence of this updraft is marked by the development of a right flank weak-echo region (WER) surmounted by a midlevel echo overhang. As this updraft develops, the maximum echo-top height

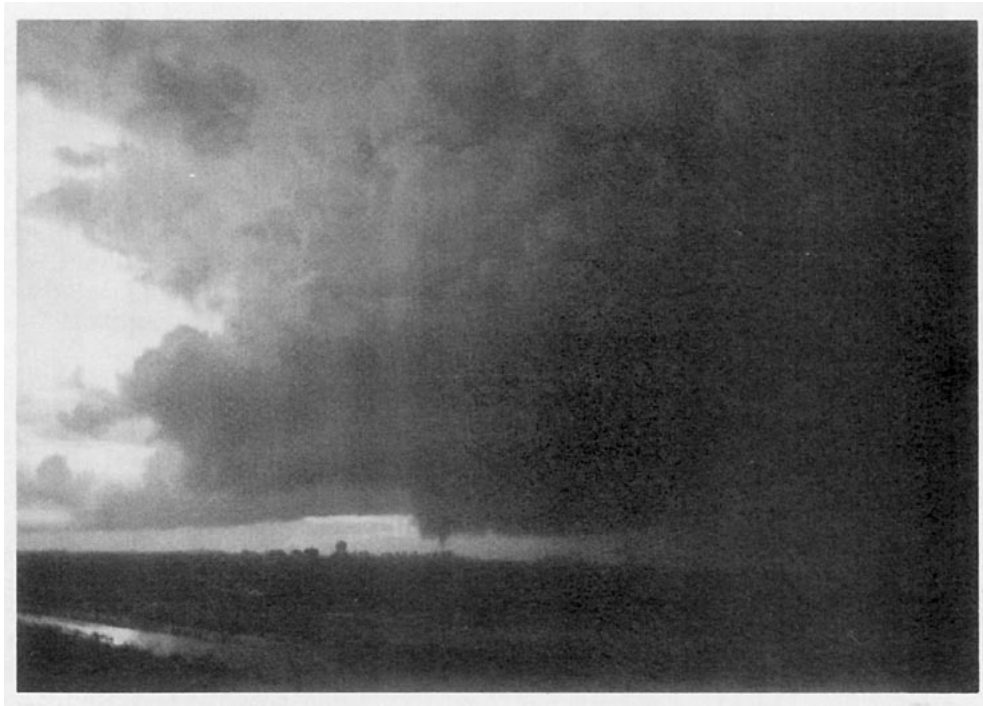

FIG. 6. Photograph of the tornado and the right flank of the parent thunderstorm. The view is toward the northwest. At the time of the photograph, the storm was located near Bement, Illinois, (photograph by William Chapman).

often increases and the echo-summit location shifts to a position above the WER. Also, a midlevel mesocyclone circulation begins to develop centered on this intensifying updraft. The storm motion frequently begins to deviate to the right of the layer mean wind direction during this phase of the supercell.

3) During approximately the next 30 min, the mesocyclone circulation intensifies as it increases in vertical extent. Radar-detectable particles swept up in this circulation may initially form a bounded weak-echo region (BWER) aloft and subsequently a hook echo near the surface.

4) During the final collapsing stage of the supercell, the midlevel echo overhang descends and eliminates the WER–BWER structures. The maximum echo-top height decreases in concert with descent of the midlevel overhang. As the low-altitude mesocyclone circulation strengthens, the hook echo may "wrap up" and become ill defined. Tornadogenesis is most probable when the mesocyclone circulation reaches its peak intensity at near surface heights.

A series of radar data analyses were performed to compare the life cycle of the Bement storm to that of a classic supercell. The data were collected by the Illinois State Water Survey–National Science Foundation CHILL radar in support of the PACE 89 (Precipitation Augmentation for Crops Experiment 1989) research project (Changnon et al. 1991). The operating characteristics of the CHILL are summarized in Table 2. During the evening of the tornado event, the radar was conducting a series of sequential 360° PPI scans at 1° elevation steps up to the echo top. The time required to complete a volume scan increased from 2 to 6 min as the storm approached the radar.

For this study, CHILL data from 1840 to 2042 were examined. The Bement tornado's parent thunderstorm echo was continuously observed throughout this period. Four volume scans representing various stages during the latter half of the storm's lifetime were selected for detailed analyses. Interactive editing of these datasets was done using the Research Data Support System (RDSS, Oye and Carbone 1981). To examine the storm's volumetric reflectivity structure, the SPRINT (sorted position radar interpolation; Mohr et al. 1981) software was used to perform a bilinear interpolation of the edited data to a 500-m resolution three-dimensional Cartesian grid. No range averaging was done before the interpolation. The gridded data were shifted

TABLE 2. CHILL radar operating characteristics on 19 May 1989.

Wavelength (cm)	10.7
Half-power beamwidth (deg)	0.96
Peak transmitted power (kW)	641
Noise power at SNR = 1 (dBm)	−110.29
Range resolution (m)	300
Unambiguous velocity (m s^{-1})	26.42
Pulses per integration cycle	50

to account for storm motion during the volume scan time intervals by the CEDRIC (custom editing and display of reduced information in Cartesian space; Mohr and Miller 1983) program.

Due to the small size of the tornadic Doppler signature, radial velocity patterns were examined using plan position indicator (PPI) plots of the individual range gate values. This data presentation method bypassed the smoothing that inevitably accompanies spatial interpolation.

Three of the four analyzed volumes have been selected to characterize the echo morphology of the Bement storm. The 1910:50 volume, some 50 min before tornado formation, represents the storm's initial configuration (Fig. 7a). It is apparent that the tornadic echo was remarkably small. The low-level area enclosed by the 45-dBZ contour averaged only 5–6 km in diameter throughout the lifetime of the storm. At 1910:50, the reflectivity horizontal gradients were not well organized. The echo-summit height was quite low (5.5 km MSL), and the top was located close to the low-altitude reflectivity core position.

The radial velocity pattern at 1910:19 suggested the presence of a somewhat disorganized cyclonic rotation couplet near the 2-km height ($x = -59.5$, $y = -15$ km), west of the 55-dBZ reflectivity core (Fig. 7b). At 1911, the storm was observed to produce a funnel cloud. Later volume scans showed that this particular rotational feature was transitory. This sequence, in which short-lived funnel cloud and tornado activity occurs before a storm achieves a high degree of supercell organization, was similar to that reported by Burgess and Donaldson (1979).

By 1938:22, indications of an updraft on the storm's right flank became evident (Fig. 8a). At this time, several of the 1.5-km reflectivity contours formed a concave inflow notch ($x = -44$, $y = -16.5$ km). A north–south vertical cross section along $x = -44$ km (Fig. 10a) showed the existence of an elevated echo overhang above the inflow WER. In addition, the strong vertical gradient of reflectivity between the 5.5- and 6.5-km heights above the WER suggested the presence of a vigorous updraft (Wakimoto and Bringi 1988).

A well-defined mesocyclonic velocity couplet ($x = -44.2$, $y = -16.3$ km) was present in the 1937:38 2.2° elevation PPI sweep (Fig. 8b). This circulation appeared to be essentially centered on the updraft responsible for the midlevel echo overhang seen in Fig. 10a. Examination of additional PPIs at other elevation angles (not shown) indicated that between 1922 and 1938, the vertical extent of the rotational couplet had increased so that the circulation spanned the 1–3-km MSL height range. Despite the presence of this developing circulation, no well-defined BWER was observed.

The collapse of the Bement storm was in progress at 2007:50 (Fig. 9a). By this time, the echo summit had subsided to a height of 5 km and the location of the top had shifted downwind of the right flank of the storm. The altered structure in the storm's right flank is depicted in a vertical cross section at $x = -28.5$ km

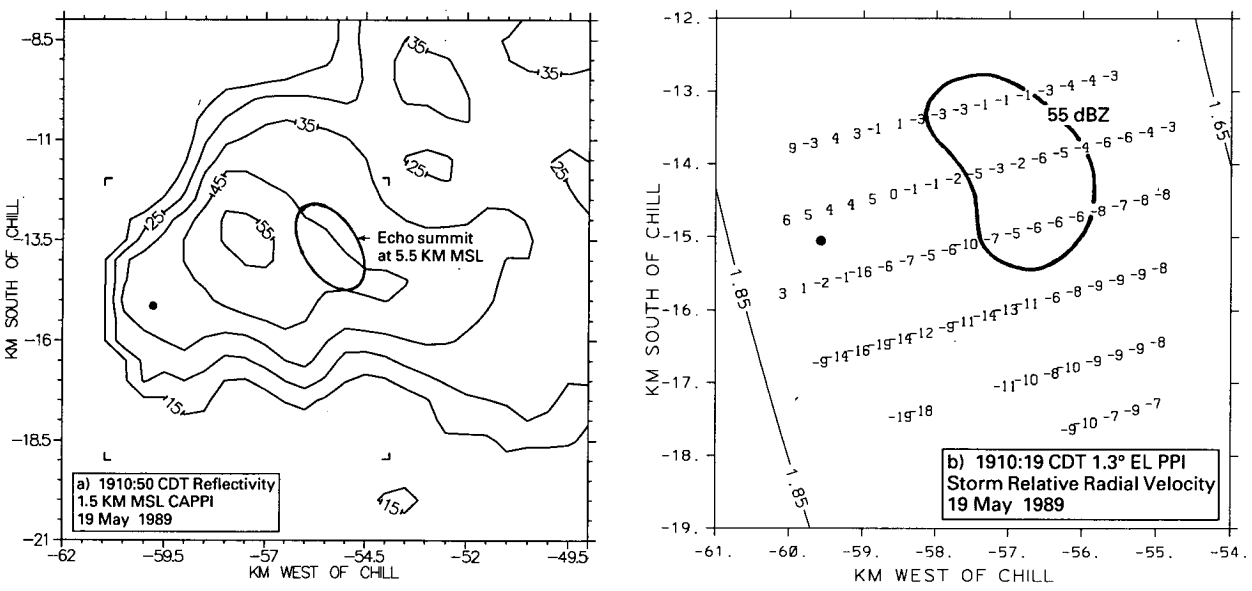

FIG. 7. CHILL radar data: presupercell stage. (a) Reflectivity CAPPI at 1.5 km MSL at 1910:50 CDT 19 May 1989. Contours start at 15 dBZ with a 10-dB increment. A tracing of the echo summit location is indicated by the heavy line. The dot marks the approximate center of the low-level circulation detected in the Doppler data. The four right-angle marks indicate the corners of the domain shown in associated radial velocity plot [panel (b)]. (b) Individual range gate storm-relative radial velocity PPI at 1910:19 CDT 19 May 1989. Elevation angle is 1.3°; velocities are in meters per second with negative values indicating flow toward the radar. Gate spacing is 300 m in range and 0.88° in azimuth. The dot marks the approximate center of the mesocyclone circulation. The heavy line traces the 55-dBZ reflectivity contour from the same PPI sweep. Solid contours are beam heights in kilometers MSL.

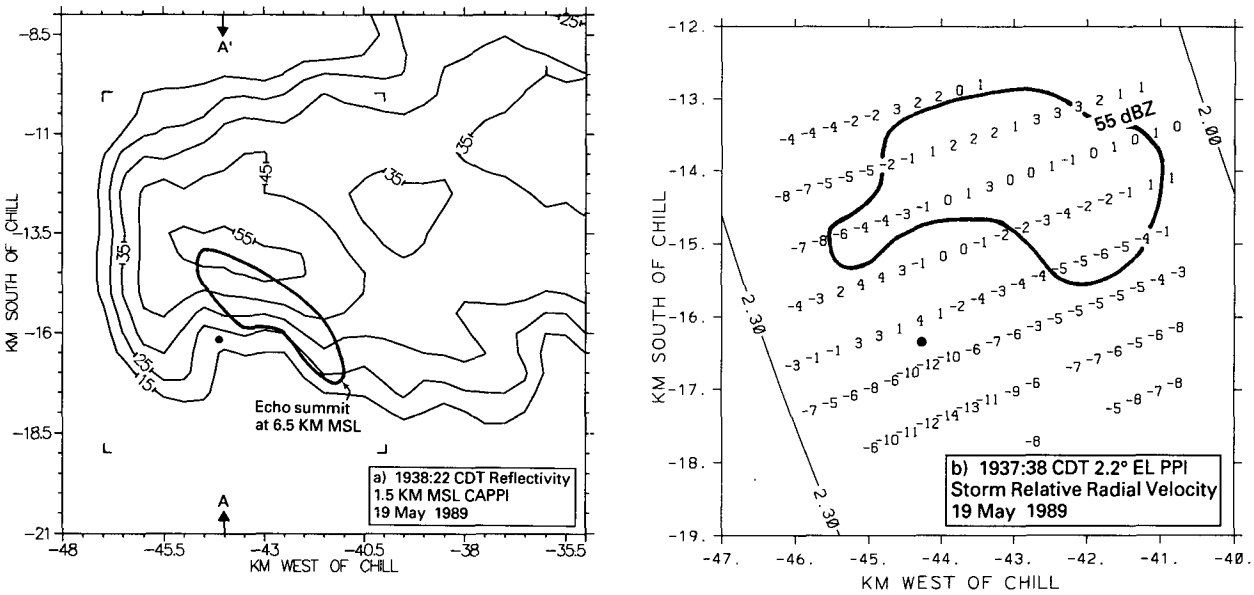

FIG. 8. CHILL radar data: supercell stage. (a) As in Fig. 7a except the time is 1938:22 CDT. The points marked A and A' locate the cross section shown in Fig. 10a. (b) As in Fig. 7b except the time is 1937:38 and the elevation angle is 2.2°.

(the mesocyclone location) at 2007:50 (Fig. 10b). Between 1938 (Fig. 10a) and 2008 (Fig. 10b), it is evident that the midlevel overhang had descended significantly and the height of the WER had diminished.

By 2006:00, the strongest mesocyclone circulation ($x = -28.5$, $y = -15.2$ km) was found at a height just above 1 km (Fig. 9b); whereas at 1938, the circulation maximum had been located near the 3-km level. The mesocyclone circulation had intensified during this descent. There was also some suggestion in this PPI that the 55-dBZ reflectivity contour began to wrap around the west side of the mesocyclone by 2006. Public reports indicate that the tornado touchdown occurred at approximately 2008 during the latter stages of the mesocyclone descent and intensification.

A summary of the vortex history is shown in a time–

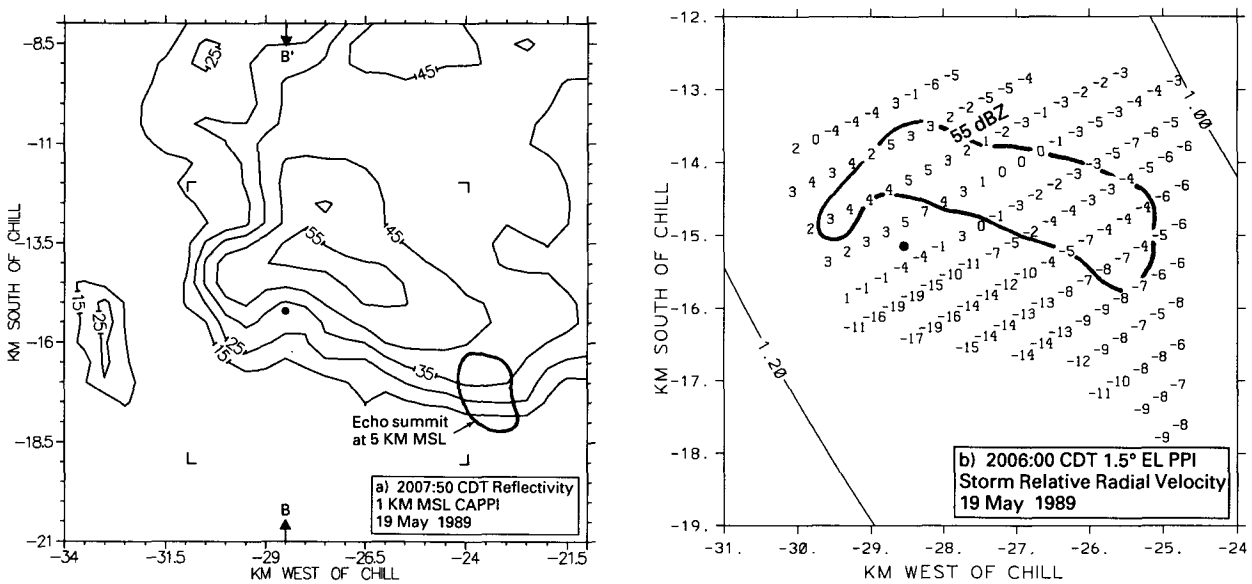

FIG. 9. CHILL radar data: collapsed supercell stage. (a) As in Fig. 7a except the time is 2007:50 CDT and the CAPPI height is 1 km MSL. The points marked B and B' locate the cross section shown in Fig. 10b. (b) As in Fig. 7b except the time is 2006:00 CDT and the elevation angle is 1.5°.

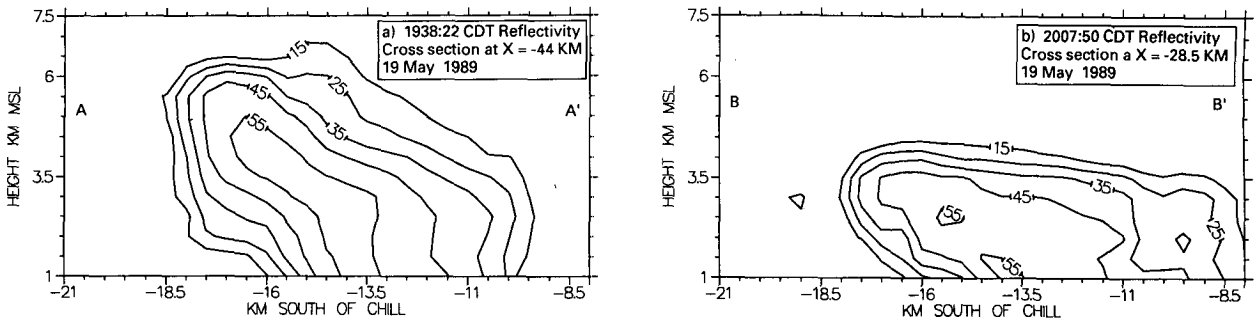

FIG. 10. CHILL radar vertical cross sections. (a) North–south vertical cross section at 1938:22 CDT 19 May 1989 along $x = -44$ km. Contours are reflectivities starting from 15 dBZ with a 10-dB interval. Heights are in kilometers MSL. (b) As in 10a except the time is 2007:50 CDT and the cross section is located at $x = -28.5$ km.

height cross section of the maximum azimuthal radial velocity shear normalized to a 25-km range (Fig. 11). Rotation developed near the midlevel of the echo and descended with time. The DEC funnel cloud sighting at 1912 occurred when an early shear maximum appeared aloft; no reports were found relating to the second period of shear intensification aloft around 1930. The reported tornado activity occurred in association with the descent of the 40 $\times$ 10^{-3} s^{-1} shear envelope to near-surface heights that began just after 2000. It should be noted that the tendency observed in this case for both the top and the base of the maximum shear envelope to descend with time was different from the behavior often seen in Oklahoma-area storms. In these latter storms, the azimuthal shear signature typically reached a maximum at all observed heights as the visible tornado diameter neared a peak (Brown et al. 1978). Thus, unlike the Oklahoma cases, the azimuthal

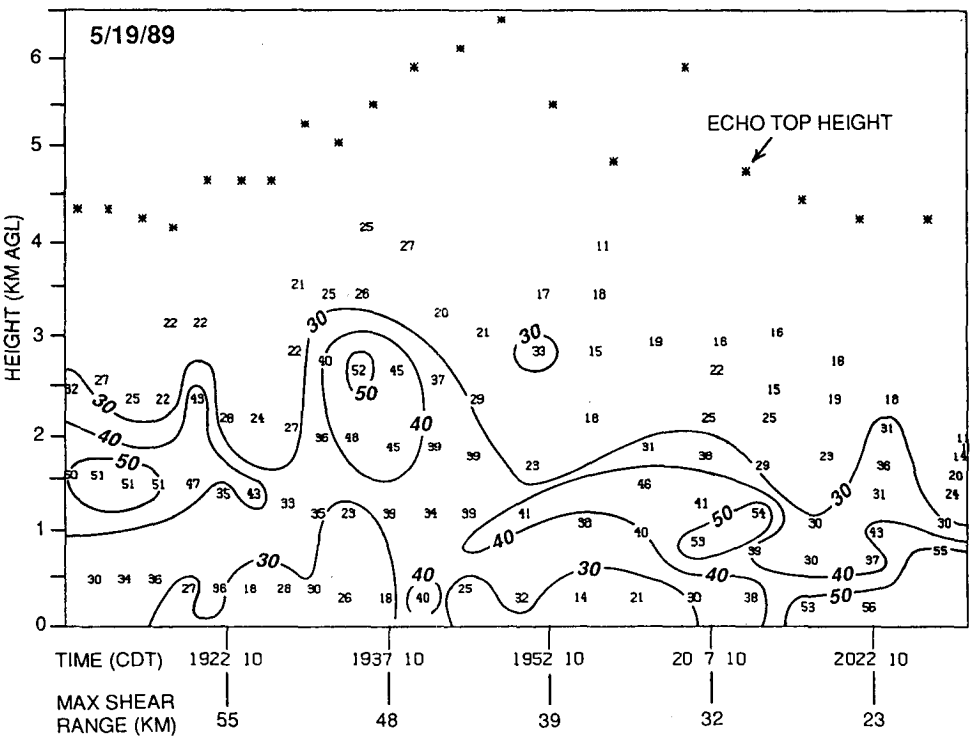

FIG. 11. Time–height plot of maximum radial velocity shear between adjacent-beam range gates. Shears have been normalized to a range of 25 km, units are 10^{-3} s^{-1}. The range normalization was accomplished by multiplying the raw shear values calculated from the basic gate data by the quantity [gate range (km)/25]. Heights are in kilometers AGL; the elevation of the radar site is 230 m. Echo-top heights are indicated by asterisks.

shear signature of the Bement tornado was collapsing toward its minimum vertical extent as the tornado was touching down.

Despite being roughly half the size of a typical supercell, the Bement storm displayed a number of supercell life-cycle characteristics: the storm existed for some 2.5 h, showed several indications of both the growth and decay of a strong right-flank updraft, and developed an elevated mesocyclone that subsequently descended prior to tornado touchdown.

4. Discussion and conclusions

From the forecasting perspective summarized by Table 1, the synoptic-scale patterns associated with the Bement tornado were not those of a classic spring season Midwest severe thunderstorm day. The synoptic-scale support for convective activity was best organized more than 100 km east of the tornado location. Of all the severe weather parameters examined in this study, only the relatively small BRI values calculated from the PIA sounding (23–45) appeared to be threatening. In typical severe weather environments, these low BRI values result from a combination of large CAPE and strong wind shear. In the PIA sounding of this case, however, both CAPE and wind shear were relatively weak so that their ratio resulted in a deceptively low BRI.

The synoptic setting was also dissimilar from those noted in cases of "cold-air funnels." Cooley (1978) reported that these funnels generally occurred several hundred kilometers to the rear of surface cold fronts beneath areas of significantly cold air aloft. Neither of these characteristics applied to this storm environment.

The NWS severe weather forecasters recognized the marginal nature of the situation. During the afternoon hours, Illinois was placed in a slight risk area for severe thunderstorms due to the interaction of the passing 500-mb vorticity lobe and diurnal heating. At 1650, the mesoscale discussion issued by the National Severe Storms Forecast Center was directed toward the developing line of thunderstorms along the Illinois–Indiana border; no tornado watch was in effect when the Bement tornado occurred.

Besides the unusual setting in which the Bement tornado occurred, several of the storm's radar characteristics were also noteworthy: The cell was quite small in size; the perimeter of the convective portion of the parent echo, as defined by the 25-dBZ contour, was only some 15 km in diameter. This is approximately half the typical tornadic echo diameter reported by Forbes (1981). The radius of the mesocyclone associated with the Bement tornado (1–2 km) was also somewhat smaller than the 2.5–3-km mesocyclone radii that are most frequently observed in Oklahoma-area storms (JDOP staff 1979). The Bement storm's maximum echo-top height also failed to reach the tropopause and instead remained between 5 and 6.5 km MSL. Owing to these limited size attributes, the parent echo and its internal circulation appeared insignificant when the full range (150 km) of the CHILL radar was displayed.

Within this small echo, both radar and visual data indicated that a number of supercell characteristics were present. Based upon the CHILL radar observations, the parent storm existed for at least 2 h. During the latter half of this period, the three-dimensional echo structure followed much of the evolutionary pattern normally seen in more classically sized supercells: In particular, the development and decay of a right flank overhang in the Bement storm's reflectivity structure indicated that a fairly strong, persistent updraft preceded tornado formation. The life cycle of the mesocyclone associated with this updraft was also similar to that observed in the southern plains (JDOP staff 1979) in that the cyclonic shear first intensified aloft and then approached the surface prior to the tornado touchdown. In keeping with the limited stature of the echo, however, the "midlevel" circulation in this case intensified near 3 km MSL, in contrast to the approximately midtropospheric heights (5–6 km) often noted in the southern Great Plains storms. The shear magnitudes were approximately half those found in strong southern plains tornadoes; the range-normalized 40–55 $\times 10^{-3}$ s^{-1} adjacent gate shears were closer to the intensities observed in Colorado events (Wakimoto and Wilson 1989).

It has been established that some, usually not major, tornadoes are produced by echoes that lack the prominent size and organizational characteristics of classic supercells (Burgess and Donaldson 1979; Bluestein and Parks 1983; Moller and Ely 1985; McCaul 1987; Wakimoto and Wilson 1989). These storms, which depart from the classic supercell echo appearance, pose a challenge for many automated Doppler radar tornado-detection algorithms.

The Bement storm provides a detailed example of the nature of the reflectivity and radial velocity patterns involved in one such atypical tornado event. In this case, neither the synoptic setting nor the full range surveillance view of the parent echo appeared threatening. Owing to the limited depth of the echo, Doppler detection of the circulation pattern at long ranges could easily be compromised by beam overshooting. Even if properly resolved, the limited vertical extent of the echo might cause some mesocyclone identification algorithms to reject this small feature. Thus, full utilization of spotter reports and magnified radar base-data display capabilities will continue to be important even after the implementation of automated Doppler-based severe weather detection algorithms.

Acknowledgments. Dr. E. A. Mueller and Mr. D. A. Brunkow of Colorado State University provided consultation and software support in the analysis of the CHILL radar data. The anonymous reviewers of this

note suggested a number of significant improvements. Information shared by personnel from the University of Illinois Department of Atmospheric Science is also acknowledged: William Chapman provided his tornado intercept photographs and observations and Harold Brooks summarized the results of his damage survey. John Brother, Jr., of the Illinois State Water Survey provided assistance in the drafting of the figures. This research was originally supported by the CHILL radar NSF Grant ATM 83-20095 and by the NOAA Precipitation Augmentation for Crops Experiment (PACE) Grant COMM NA89RAH07077. Patrick Kennedy is currently supported by the CSU–CHILL NSF cooperative agreement ATM-89 19080. Nancy Westcott and Robert Scott are supported by the Atmospheric Modification Program under NOAA cooperative agreement COMM NA27RA-0173-01.

REFERENCES

Bluestein, H. B., and C. R. Parks, 1983: A synoptic and photographic climatology of low-precipitation severe thunderstorms in the southern plains. *Mon. Wea. Rev.*, **111,** 2034–2046.

Burgess, D. W., and R. J. Donaldson, Jr., 1979: Contrasting tornadic storm types. Preprints, *11th Conf. Severe Local Storms,* Amer. Meteor. Soc., Kansas City, 189–192.

——, and L. R. Lemon, 1990: Severe thunderstorm detection by radar. *Radar in Meteorology,* D. Atlas, Ed., Amer. Meteor. Soc., 619–647.

Changnon, S. A., R. R. Czys, R. W. Scott, and N. E. Westcott, 1991: Illinois precipitation research: A focus on cloud and precipitation modification. *Bull. Amer. Meteor. Soc.,* **72,** 587–604.

Cooley, J. R., 1978: Cold air funnel clouds. *Mon. Wea. Rev.,* **106,** 1368–1372.

Davies, J., 1990: Midget supercell spawns tornadoes. *Weatherwise,* **43,** 260–261.

Davies-Jones, R., D. W. Burgess, and M. Foster, 1990: Test of helicity as a tornado forecast parameter. Preprints, *16th Conf. Severe Local Storms,* Kananaskis Park, Alberta, Canada, Amer. Meteor. Soc., 588–592.

Forbes, G. S., 1981: On the reliability of hook echoes as tornado indicators. *Mon. Wea. Rev.,* **109,** 1457–1466.

——, and R. M. Wakimoto, 1983: A concentrated outbreak of tornadoes, downbursts and microbursts, and implications regarding vortex classification. *Mon. Wea. Rev.,* **111,** 220–235.

Fujita, T. T., 1981: Tornadoes and downbursts in the context of generalized planetary scales. *J. Atmos. Sci.,* **38,** 1511–1534.

Hoskins, B. J., I. Draghici, and H. C. Davies, 1978: A new look at the omega equation. *Quart. J. Roy. Meteor. Soc.,* **104,** 31–38.

JDOP staff, 1979: Final report on the Joint Doppler operational Project (JDOP) 1976–1978. NOAA Tech. Memo., ERL NSSL-86, Norman, OK, 84 pp.

McCaul, E. W., Jr., 1987: Observations of the Hurricane "Danny" tornado outbreak of 16 August 1985. *Mon. Wea. Rev.,* **115,** 1206–1223.

Maddox, R. A., and C. A. Doswell III, 1982: Forecasting severe thunderstorms: A brief evaluation of accepted techniques. Preprints, *12th Conf. Severe Local Storms,* San Antonio, Amer. Meteor. Soc., 92–95.

Miller, R. C., 1972: Notes of analysis and severe storm forecasting procedures of the Airforce Global Weather Central. Tech Rep. 200 (Rev) AWS, U.S. Air Force,

Mohr, C. G., and L. J. Miller, 1983: CEDRIC—A software package for Cartesian space editing, synthesis and display of radar fields under interactive control. Preprints, *21st Radar Meteorology Conf.,* Edmonton, Alberta, Canada, Amer. Meteor. Soc., 569–574.

——, ——, and R. L. Vaughan, 1981: An interactive software package for the rectification of radar data to three-dimensional Cartesian coordinates. Preprints, *20th Radar Meteorology Conf.,* Amer. Meteor. Soc., Boston, 690–695.

Moller, A. R., 1978: The improved NWS storm spotters' training program at Fort Worth, Texas. *Bull. Amer. Meteor. Soc.,* **59,** 1575–1582.

——, and G. Ely, 1985: On the operational problem of warning for the anomalous severe weather event: The Dallas county tornado of 13 December 1984. Preprints, *14th Conf. on Severe Local Storms,* Amer. Meteor. Soc., Indianapolis, 346–349.

Oye, R., and R. Carbone, 1981: Interactive Doppler editing software. Preprints, *20th Radar Meteorology Conf.,* Boston, Amer. Meteor. Soc., 683–689.

Ray, P. S., 1990: Convective dynamics. *Radar in Meteorology,* D. Atlas, Ed., Amer. Meteor. Soc., 348–390.

Wakimoto, R. M., and V. N. Bringi, 1988: Dual-polarization observations of microbursts associated with intense convection: The 20 July storm during the MIST Project. *Mon. Wea. Rev.,* **116,** 1521–1539.

——, and J. W. Wilson, 1989: Non-supercell tornadoes. *Mon. Wea. Rev.,* **117,** 1113–1140.

Weisman, M. L., and J. B. Klemp, 1984: The structure and classification of numerically simulated convective storms in directionally varying wind shears. *Mon. Wea. Rev.,* **112,** 2479–2498.